Selectivity filter mutations shift ion permeation mechanism in potassium channels

Andrei Mironenko[1], Bert L. de Groot[1], Wojciech Kopec[1]

[1]Computational Biomolecular Dynamics Group, Max Planck Institute for Multidisciplinary Sciences, Am Fassberg 11, 37077 Göttingen, Germany

Corresponding author: Wojciech Kopec, Am Fassberg 11, 37077 Goettingen, Germany, +49 551 201-2306, wojciech.kopec@mpinat.mpg.de

Preprint Server: bioRxiv

Classification: Physical Sciences, Biological Sciences, Biophysics and Computational Biology

Keywords: Potassium Channels, Molecular Dynamics, Ion Permeation, Permeation Mechanisms

Abstract

Potassium (K^+) channels combine high conductance with high ion selectivity. To explain this efficiency, two molecular mechanisms have been proposed. The ‘direct knock-on’ mechanism is defined by water-free K^+ permeation and formation of direct ion-ion contacts in the highly conserved selectivity filter (SF). The ‘soft knock-on’ mechanism involves co-permeation of water and separation of K^+ by water molecules. With the aim to distinguish between these mechanisms, crystal structures of two SF mutants in the KcsA channel - G77 and T75 - were published, where the arrangements of K^+ ions and water display canonical soft knock-on configurations. These data were interpreted as evidence of the soft knock-on mechanism in wild-type channels (C. Tilegenova, *et al.*, Structure, function, and ion-binding properties of a K+ channel stabilized in the 2,4-ion–bound configuration. *Proceedings of the National Academy of Sciences* **116**, 16829–16834 (2019)). Here, we test this interpretation using molecular dynamics simulations of KcsA and its mutants. We show that, while a strictly water-free direct knock-on permeation is observed in the wild-type, conformational changes induced by these mutations lead to distinct ion permeation mechanisms, characterized by a co-permeation of K^+ and water. These mechanisms are characterized by reduced conductance and impaired potassium selectivity, supporting the importance of full dehydration of potassium ions for the hallmark high conductance and selectivity of K^+ channels. In general, we present a case where mutations introduced at the critical points of the permeation pathway in an ion channel drastically change its permeation mechanism in a non-intuitive manner.

Significance statement

Potassium (K+) channels exhibit exceptional efficiency and selectivity in conducting potassium ions. Elucidating the molecular mechanisms that govern ion conduction is crucial for understanding K+ channels. In this study, we investigate the effects of two mutations introduced in the highly conserved functional core - the selectivity filter - of a model K+ channel KcsA using molecular dynamics simulations. We demonstrate that these mutations lead to a substantial decrease in conductance and compromised ion selectivity, which is accompanied by a shift from water-free K+ permeation to co-permeation with water molecules. Our findings provide a fundamental example of how single point mutations in the selectivity filter alter the permeation mechanism, and reinforce the notion that water exclusion underlies the remarkable efficiency of K+ channels.

Introduction

Potassium channels (K^+ channels) enable the permeation of K^+ ions along their electrochemical gradient across plasma and organelle membranes in almost all organisms. They play an essential role in establishing the membrane potential in living cells, terminating action potentials in excitable cells, as well as in many other physiological processes (1). K^+ channels are able to conduct K^+ with very high permeation rates, with conductances reaching hundreds of pS (2). At the same time, they possess exceptional selectivity for K^+ over other monovalent ions, with K^+/Na^+ permeability ratios reaching ~100-1000 (3). In the last decades a great effort has been put into determining the ion permeation mechanism that can explain such high K^+ permeation efficiency, combined with strict K+ selectivity.

K^+ channels possess a highly conserved selectivity filter (SF), usually having a signature sequence TVGYG (4, 5). The SF is the narrowest part of a K^+ channel pore, and serves as the functional core of the channel. It consists of 4 K^+ binding sites - S1 to S4 respectively - lined by backbone carbonyls (S1-S4) and threonine hydroxyls (S4 only), pointing toward the permeation pathway (Fig. 1*A*). The K^+ permeation mechanism in K^+ channels is defined by specific arrangements of K^+ ions and, possibly, water molecules inside SF, occuring during an ion translocation through the channel. Currently, there are two primary models of K^+ permeation in K^+ channels: the 'soft knock-on' and 'direct knock-on' mechanisms (6). Soft knock-on was proposed following the first structural data: it states that SF is occupied by 2 K^+ simultaneously - either in S1 and S3, or S2 and S4 - and by water molecules in the remaining 2 sites (7, 8). This separation of two K^+ ions by a water molecule was included to prevent seemingly too strong electrostatic repulsion between K^+ ions, if they would occupy neighboring sites. Accordingly, in the course of a permeation event, given an initial configuration 'KWKW' (K stands for a K^+ ion, and W for a water molecule, in sites S1 to S4 respectively), an ion approaching S4 from the intracellular side 'knocks on' the contents of SF to a configuration 'WKWK' (Fig. 1*A*), and vice versa - thus, for each K^+ ion there is one water molecule permeating the channel. A very different process takes place in the direct knock-on mechanism, as water does not permeate the channel. Rather, K^+ ions are completely dehydrated in the SF, and direct ion-ion contacts are formed (Fig. 1*A*) (9). This complete dehydration of K^+ ions in the SF makes ion permeation inherently selective towards K^+ compared to Na^+ (10). In addition, the strong electrostatic repulsion arising from the direct ion-ion contacts was proposed to drive fast permeation in K^+ channels (9). Importantly, both soft and direct knock-on mechanisms follow a strict single-file ion (and water) permeation and an unperturbed SF conformation is assumed during ion permeation.

In extensive experimental and computational studies of K^+ permeation mechanisms some results support soft knock-on (e.g. streaming potentials (11–13) and global fits by electrophysiology (14)), whereas others favor direct knock-on (e.g. fully occupied SF by K+ in crystal structures (5, 15, 16), i.e. 'KKKK' configuration (Fig. 1*B*), computational electrophysiology molecular dynamics simulations (9, 10) or solid-state NMR measurements (17)) (6). Thus, the debate on which mechanism actually takes place in K^+ channels remains unresolved. Within this debate, recent data on SF mutants: G77A and T75X (X=A, C, G) in the model K+ channel KcsA, present an intriguing case. The G77A mutation effectively removes the S3 binding site, as the

backbone carbonyls of V76 point away from the ion pathway (carbonyl 'flip') in the crystal structure (Fig. 1*B*) (18). Interestingly, the structure shows both S3 and S1 occupied not by K^+, but by water molecules instead (the 'WKWK' configuration). As mentioned above, one of the arguments in favor of direct knock-on is the 'KKKK' configuration in crystal structures of most WT K^+ channels. However, an alternative interpretation posits the 'KKKK' configuration as a superposition of soft knock-on 'WKWK' and 'KWKW' configurations (8) (Fig. 1*C*). In this context, the structure of G77A was originally interpreted as one isolating the 'WKWK' configuration, the same configuration that would occur during permeation in WT via the soft knock-on mechanism (18). In the same spirit, T75C and T75G mutations not only remove the S4 binding site, but lower the K+ occupancy at S2, which has been interpreted as an isolated 'KWKW' configuration (Fig. 1B) (19, 20). Interestingly, the occurrence of soft-knock on-specific configurations in G77A and T75X mutants has been taken as evidence for the soft-knock on mechanism in WT K+ channels (18). Functionally, mutations at both 75 and 77 positions largely decrease K+ conductance (ca. 32-fold for G77A (18) and between 3-17-fold for T75X (19, 21)). The data on ion selectivity are ambiguous: liposome flux assay (LFA) experiments showed WT-like K^+/Na^+ selectivity in KcsA G77A (18), whereas no selectivity measurements have been conducted (to the best of our knowledge) on T75X mutants. For other channels with the conserved SF sequence (TVGYG), the electrophysiological selectivity measurements are conflicting: hKv1.5 T480A and Shaker T442A (21) retained K^+ selectivity, while NaK2K T63A and MthK T59A were non-selective (22).

In this work, we study ion permeation mechanisms in the G77A and T75A mutants of KcsA using molecular dynamics (MD) simulations with applied voltage with two modern fixed-charge force fields. In our simulations, WT KcsA permeates strictly via water-free direct knock-on, whereas both mutations drastically affect the SF conformational dynamics, coupled with permeation mechanisms incompatible with direct knock-on. In fact, the strict water-free K^+ permeation is compromised in G77A and T75A, leading to largely reduced permeation rates, in good agreement with experimental data (18, 19, 21). The K^+/Na^+ selectivity of the mutants is similarly diminished. Our findings not only present a case when the structural and mutagenesis data should be interpreted with caution in the context of ion permeation mechanisms, but also support the idea that exclusion of water from the SF is necessary for the hallmark high conductance/high selectivity combination in K^+ channels.

Results

Ion permeation in the WT channel

First, we simulated ion conduction in WT KcsA at the membrane voltage of 300 mV, using the CHARMM36m (23) and Amber14sb (24) force fields. In simulations with CHARMM36m we observed 40 K^+ permeation events within cumulative 10us simulation time, the majority of which occurred via direct knock-on. Rarely, a water molecule entered the central parts of the SF (S2/S3). In these cases the further ion permeation was halted (*SI Fig. 1A)*, suggesting that water in the SF transiently blocks ion permeation. In one case, SF underwent drastic conformational changes with a large increase in diameter at S3, S2 and S1 that allowed

permeation of both K^+ and water (*SI Fig. 1B)*. In contrast, in Amber14sb, the SF was stable and inaccessible to water (*SI Fig. 1C*), allowing to observe 81 permeation events that occurred exclusively via direct knock-on. The calculated outward conductances are therefore 2.1 ± 1.1 pS and 4.3 ± 1.1 pS in CHARMM36m and Amber14sb, respectively, an order of magnitude lower than the experimental values for KcsA (3) - a known effect of K+ channels simulations using fixed-charge models (6).

The SF of WT KcsA in MD simulations with the CHARMM36 force field can transition toward the 'constricted' conformation, related to C-type inactivation, within hundreds of nanoseconds (25, 26). In our simulations we did not observe such transitions (*SI Fig. 2*), possibly due to lower temperature in our study, or limited sampling. We noticed that the SF was on average narrower in CHARMM36m compared to Amber14sb at G77 (by ~0.04 nm, distance between CA atoms of opposing subunits) and G79 (~0.02 nm). Our previous work on MthK channels showed that subtle changes in the SF diameter can have major effects on outward currents (27), thus it is feasible that such an effect might be present in KcsA as well (*SI Fig. 3)*.

Finally, we tested the selectivity of WT KcsA by simulating in the presence of Na+ ions (instead of K+). We did not observe any Na^+ permeation in WT KcsA using CHARMM36m, and only 2 permeation events with Amber14sb (PK^+/PNa^+ ~ 40), showing a strict K+ selectivity, in agreement with experiments (3).

Ion permeation in KcsA E71A

As the WT KcsA showed unstable K^+ permeation with low conductance, we investigated its non-inactivating E71A mutant (Si Fig 4A), to obtain a clearer picture of K^+ permeation, since earlier MD simulations showed higher currents and stability of KcsA E71A compared to WT (26). Similarly, in our simulations, KcsA E71A showed sustained currents with both force fields. K^+ permeation occurred consistently via direct knock-on (*SI Fig. 4B*). In total, we observed 494 permeation events over cumulative 10 μs of simulations with KcsA E71A in CHARMM36m (and only 3 water permeation events), and 124 in Amber14sb (no water permeation events) (*SI Table 1*) - corresponding to 26.4 ± 4.3 pS and 6.6 ± 1.4 pS respectively. The increased conductance for E71A correlates with the SF width: E71A is ~0.05 nm wider at G79 compared to WT (CHARMM36m), in line with our previous work on MthK and its KcsA-like V55E mutant (27).

At the same time, KcsA E71A retains the strict K+ selectivity: no Na^+ permeation was observed in simulations with the CHARMM36m force field, and only 3 Na^+ permeation events with Amber14sb (PK^+/PNa^+ ~ 40). Thus, KcsA E71A shows essentially the same permeation mechanism (direct knock-on) and ion selectivity as the WT channel, with much higher currents. We thus conducted our study on SF mutations in the following manner: first, we introduced the SF mutations into KcsA E71A, and investigated their effect on K^+ permeation in G77A/E71A and T75A/E71A constructs. As control systems we simulated the single G77A and T75A mutants, and compared their behavior to the 'pure' WT KcsA (that is, without the E71A mutation), to

account for possible biases of channel sequences and force fields, and get the comprehensive picture of the effect of SF mutations on ion permeation.

Effect of the G77A mutation

The introduction of G77A into KcsA E71A leads to a drastic change in the permeation mechanism: the mutated channel co-permeates water molecules, thus compromising the water-free direct knock-on mechanism (*Fig. 2A, B, middle*). Although this mechanism resembles soft knock-on, there are some differences - K+ ions permeated by jumping directly from the KW**K**W configuration to **K**WKW - without the intermediate W**K**WK that is expected according to the canonical definition of the soft knock-on mechanism (*SI Fig. 5A*). The dominance of the KWKW occupancy pattern is not compatible with electron densities in the SF of WT channels that correspond to similar ion occupancy for all four central ion binding sites (5, 15, 16), hence rendering this permeation mechanism unlikely for the WT channel. Moreover, the number of intervening water molecules between K^+ ions was often 2 or more (instead of expected 1 water molecule). Importantly, the average position of K^+ and water inside the SF in our simulations is in good agreement with the crystal structure of G77A (18) (*Fig. 2A*), with an exception of S4. In the crystal structure, S4 is occupied by a K+ ion, whereas simulations show a larger K+ density at S3 in both force fields (*Fig. 2A* and *SI Fig. 6A*). We attribute this discrepancy to V76 carbonyl flipping dynamics: in the crystal structure, all 4 V76 are flipped, while in our simulations the number of simultaneously flipped V76 ranges between 0 and 4, and conformations with a larger number of simultaneous flips are less frequent (*Fig. 3C*). Accordingly, the fraction of frames where K^+ occupies S4 instead of S3 increases with the number of simultaneously flipped V76 (*SI Fig. 6B*).

The above mentioned shift in ion permeation mechanism drastically reduces K+ conductance for G77A/E71A compared to E71A. In total, we observed only 15 permeation events in CHARMM36m, and 4 in Amber14sb, over ~20 μs and 10 μs total simulation time, respectively (*SI Table 1*), corresponding to an average ~50-fold (CHARMM36m) and ~30-fold (Amber14sb) reduction in outward conductance (*Fig. 2C* and *SI Fig. 7A*). This decrease agrees well with experimental estimates (32-fold reduction) (18). Further, K+/Na+ ion selectivity of G77A/E71A is clearly impaired in CHARMM36m, as the channel permeates Na^+ ions at a rate similar to K^+ (*Fig. 2C*). This Na^+ permeation, akin to K^+, featured water co-permeation (*Fig. 2D, SI Fig. 5B*). While the loss of ion selectivity has a straightforward explanation within the direct knock-on framework (10) (lack of complete ion desolvation reduces K+ selectivity vs Na+, due to differences in solvation free energies), it is in apparent contrast with the interpretation of the LFA experiments in which the G77A mutant does show ion selectivity (18). We address these discrepancies in the Discussion. To get a more complete comparison to the LFA measurements, where the channel is oriented randomly in the liposomal membrane, we also simulated inward permeation (at -300 mV) with CHARMM36m. Similarly to simulations at the positive voltage, G77A/E71A was equally permeable to Na^+ and K^+, while E71A retained its selectivity (*SI Fig. 7B*). In contrast, we did not observe any Na^+ permeation in simulations with Amber14 sb. Given the very low K^+ permeation rate of G77A/E71A with this force field (4 events in 10 μs), it is

difficult to conclude whether this mutant is actually selective in this force field. Control simulations of KcsA G77A without the E71A mutation also showed a water-mediated permeation mechanism, with a reduced average outward conductance compared to WT in CHARMM36m (~2-fold) (*SI Fig. 8A*). Ion selectivity was compromised in CHARMM36m at both positive and negative voltages (*SI Fig. 8B, C*). In Amber14sb, we again did not observe K^+ or Na^+ permeation, whereas flipping of V76 occurred in both force fields (*Fig. 3C*).

Effect of the T75A mutation

T75A removes the hydroxyl groups that form the bottom of the S4 ion binding site. Consequently, in the crystal structure of KcsA T75A the K^+ ion in S4 is replaced by a water molecule (21) (*Fig. 1B, right*). In our simulations of KcsA T75A/E71A, this had a dramatic effect on K+ permeation, in a force field-dependent manner. In Amber14sb, we did not observe any ion permeation, and the content of the SF nor its conformation did not change from the starting configuration (XKKX, X = W or 0) over multiple 1 μs trajectories (*SI Fig. 9*). In contrast, in CHARMM36m, the introduction of the T75A mutation leads to co-permeation of K^+ and water (*Fig. 2A, right, SI Fig. 10*). Interestingly, while in the crystal structure of KcsA T75A carbonyls of V76 are not flipped, we observe a tendency of T75A/E71A to flip at V76, in a similar manner to G77A/E71A and G77A (*Fig 3A-C).* Flipping correlated with water entry into the SF, suggesting that it could be a general feature of water-filled selectivity filters (*Fig. 3D, SI Fig. 12C*).

KcsA T75A/E71A in CHARMM36m shows a low outward K^+ conductance of 0.5 ± 0.2 pS (*Fig. 2C*) (10 permeation events over 10 μs), which is in good agreement with experiments (21). Further, the mutant is equally permeable to K^+ and Na^+ (*Fig. 2C*), suggesting compromised ion selectivity. We cannot compare this prediction with experiments, as ion selectivity measurements are lacking for KcsA T75X constructs, and the data for other K+ channels are inconclusive (see Introduction).

In control simulations of KcsA T75A without the E71A mutation, we also observed low K^+ conductance of 0.40 ± 0.16 pS (15 K^+ permeation events over 20 μs) with CHARMM36m, (*SI Fig. 11A*), and no ion permeation with Amber14sb. The permeation mechanism was generally similar to that of T75A/E71A, featuring a co-permeation of water and K^+. The double mutant shows a preference for a stepwise motion of the KWK pair through the SF, while in T75A direct jumps from KW**K**W to **K**WKW occur, without the intermediate configuration W**K**WK (*SI Fig. 11B*). Again, this is at odds with the original soft knock-on mechanism that requires KWKW and WKWK to occur with similar probabilities, in order to explain the similar electron densities at the four central ion binding sites in the SF of non-mutated channels. Interestingly, the resulting K^+ density profile displays a relatively diminished K^+ density at S2 compared to the double mutant (*SI Fig. 13*), reminiscent of the crystal structure of KcsA T75C and T75G (19, 20). The frequency of V76 flipping was higher compared to the double mutant *(Fig. 3C*), suggesting that K^+ ions are interacting weaker with the S2-forming V76 carbonyls, in line with the decreased K^+ density at S2 in T75A. Regarding ion selectivity, only 1 Na^+ permeation event over the total 20 μs of

simulation was detected (conductance of 0.027 ± 0.06 pS), suggesting decreased ion selectivity as compared to WT, which was completely impermeable to Na+ ions.

Discussion

In this work, we studied the effect of the G77A and T75A mutations on ion permeation mechanism and selectivity in the model potassium channel KcsA channel using MD simulations with applied voltage, using two popular force fields. We show that the introduction of these mutations leads to a complete change of the K^+ permeation mechanism - from a water-free direct knock-on to mechanisms that feature a co-permeation of water. This, in turn, dramatically reduces ion permeation rates, in a good agreement with experimental data. Importantly, we introduced mutations into the SFs of both WT KcsA and its non-inactivating E71A variant; the observations of the shift towards water-mediated permeation mechanisms and low conductance are solely due to the introduced mutations and independent of the initial channel.

The shift in the permeation mechanism is rationalized by the altered conformational landscape of mutated SFs. In the crystal structure of KcsA G77A, S2- and S3-forming V76 carbonyls are in the flipped state as they point away from the pore axis (18) (*Fig. 1B, middle*). This V76 flipping occurs spontaneously in our simulations of G77A/E71A (and G77A). In contrast to the crystal structure however, not all 4 V76 are simultaneously flipped throughout the simulations, but rather the number of flipped carbonyls fluctuates between 0 and 4. The details of carbonyl dynamics vary between the systems (with or without the E71A mutation) and the force field used (*Fig. 3C*). These differences may be explained by the fact that the crystal structure was solved with an imposed four-fold symmetry and also at a lower temperature (100 K) than our simulations (290 K). Consequently, low energetic barriers between flipped/non-flipped states are crossed. Notably, this carbonyl dynamics directly affects the position of the lower ion in the SF, as it is more often located in S4 (i.e. its crystallographic site) when more V76 are simultaneously flipped (*SI Fig. 6B*).

Unexpectedly, we observed a similar behavior in the T75A mutant. Even though it only removes the hydroxyl groups of the S4-forming T75 residue, and otherwise does not affect SF conformation in the crystal structure (*Fig. 1B, right*) (21), we observed flipping of V76 carbonyls in simulations of T75A as well. For all systems we studied, we found a clear correlation between V76 flipping and water entrance into the K^+ binding sites formed by V76, that is S2 and S3 (*SI Fig. 12C, Fig. 3D*). Similar correlation between the water presence in the SF and flipping of S2/S3 carbonyls was demonstrated in previous MD studies of MthK (28), TREK-2 (29) and HERG (30) channels. In our simulations, water molecules formed hydrogen bond networks with carbonyl oxygens, and these interactions appear to stabilize carbonyls in a specific state (flipped or not flipped), depending on the instantaneous configuration of the network (*SI Fig. 12D*). However, the non-flipped orientation occurred also in the absence of these hydrogen bonds (*SI Fig. 12E*). Moreover, specific orientations of a water molecule, with its oxygen atom pointing toward a carbonyl oxygen, could induce flipping of such carbonyl, due to local electrostatic repulsion (*SI Fig. 12D)*. Taken together, carbonyl flipping is likely affected by a

combination of factors, such as the absence of ions (*SI Fig. 6B*), presence and configuration of water molecules in S2/S3, as well as the sequence and conformation of the SF and the regions behind it (*Fig. 3C*).

The exquisite ion selectivity of K+ channels arises from a balance of interactions between ions, water and the selectivity filter. We have previously shown that the direct knock-on mechanism is intrinsically selective for K^+ against Na^+, due the difference in ion dehydration free energies (10), therefore we expected a diminished ion selectivity for the water permeating mutants. In line with these expectations, mutants of other K^+ channels at the second glycine in the SF (corresponding to G77 in KcsA), i.e. BK G354S (31), GIRK2 G156S (human G154S) (32, 33) and Shaker G376A (4), show a loss of ion selectivity in electrophysiology. On the contrary, LFA measurements of KcsA G77A suggested that G77A in KcsA conserves ion selectivity (18). In our simulations both G77A and G77A/E71A are clearly non-selective in CHARMM36m, at both positive and negative voltages. With Amber14sb these mutants did not display any Na^+ permeation, but also K^+ conductance was very low (i.e. only 4 permeation events in 10 μs for G77AE71A, and G77A was non-conductive), which prevented us from making conclusions about their ion selectivity with this force field. One possible reason for this discrepancy between LFA experiments and MD simulations could be the different driving forces of ion permeation: while an applied electric potential was used in our study, in LFA ions are driven in or out of liposomes by their concentration gradients. This can lead to uncertainty in the instantaneous transmembrane voltage. Second, the intracellular cavity of KcsA was shown to be blocked by Na^+ in a voltage-dependent manner (34). Na^+ block can be relieved either by diffusion of Na^+ back into the intracellular solution, or via a 'punchthrough' mechanism through the SF by incoming ions; however, it is not clear to what extent this phenomenon is present for KcsA in LFA and how it would affect the results. Finally, the method showed an overall higher current for K^+ compared to Na^+ in this setup, but did not preclude Na^+ currents, nor quantify the effect of G77A on ion selectivity. In this vein, a possible interpretation of the LFA results that could be reconciled with our MD data is that even if KcsA G77A possesses some preference for K^+ against Na^+, the selectivity is still diminished compared to WT, as it is the case for the mutants of the glycine of BK (PK^+/PNa^+ ~ 5) (31), GIRK (~1.3) (32, 33) and Shaker (~1.2) (4) channels.

Notably, mutations of the S3 glycine in K^+ channels in humans can cause disorders such as progressive cerebellar ataxia (BK G354S (31)) and Keppen-Lubinsky syndrome (GIRK2 G154S (35)). As mentioned above, these mutants have diminished conductance and ion selectivity, and in a previous MD study of GIRK2 G154S a water-mediated K^+ permeation was reported (36). Taken together with our results, it is plausible that a shift in ion permeation mechanism underlies disease phenotypes, providing a mechanistic basis for these diseases that may guide future development of drugs.

The T75A mutation behaved similar to G77A in our simulations: it displayed reduced selectivity for K^+ (for both single and double mutation) in CHARMM36m at positive voltage (we did not observe any K^+ or Na^+ permeation for either system at negative voltage nor with Amber14sb), with identical K^+ and Na^+ conductances in T75A/E71A, and somewhat higher conductance for K^+ in T75A (*Fig. 2C, SI Fig. 11A*). As mentioned, we are not aware of ion selectivity

measurements for KcsA T75A. However, the ion selectivity measurements of other K^+ channels with mutated threonine at the same location are conflicting: Kv1.5 T480A and Shaker T442A mutants were selective (21), while NaK2K T63A and MthK T59A were non-selective (22). This channel-dependent effect of the SF threonine substitution can indicate channel-dependent shift in the ion permeation mechanism, posing an intriguing question - do selective mutants conserve the WT permeation mechanism, while non-selective ones have it switched to a non-WT mechanism, similarly to what we observed for KcsA T75A?

Recently, the fact that crystal structures of G77A and T75X mutations of KcsA show ion/water configurations of their SFs has been interpreted as evidence for the soft knock-on mechanism in WT channels as well (18). In this context, the 'KKKK' configuration found in SFs of WT channels is viewed as a superposition of 'WKWK' and 'KWKW' configurations (characteristic for soft knock-on, *Fig 1A*). Consequently, KcsA G77A has been proposed to isolate 'WKWK', whereas KcsA T75X would isolate 'KWKW', as T75X showed a decreased K^+ density at S2 (on top of eliminating S4). This presents an argument in favor of soft knock-on in WT KcsA, under a critical assumption that the permeation mechanism is not affected by the introduced mutations. Our results, however, show that both mutations largely perturb the conformational landscape of the SF, to an extent that makes the permeation mechanism in the mutants incompatible with that of the WT. Thus, we argue the experimental data on KcsA G77A and T75X do not contradict the direct knock-on mechanism in unperturbed K^+ channels. Instead, G77A and T75X simply conduct ions (and water) via an entirely different mechanism. The water-free K^+ permeation within the direct knock-on framework as a prerequisite for combined high conductance and selectivity of K^+ channels is supported by several studies, both computational and experimental (6), and our current results fit very well within this framework, thus further solidifying direct knock-on as the permeation mechanism in K^+ channels.

Materials and Methods

System preparation

The starting structure for KcsA non-inactivating mutant E71A in the open conformation (PDB ID: 5vk6 (37)) embedded in a lipid bilayer was built using CHARMM-GUI (38, 39). N- and C-termini were acetylated and methylamidated, respectively. The system contained 39 1,2-dioleoyl-sn-glycero-3-phospho-(1'-rac-glycerol) (DOPG) and 105 1,2-dioleoyl-sn-glycero-3-phosphoethanolamine (DOPE) molecules in the lipid bilayer; 11257 water molecules; 163 K^+ and 140 Cl^- ions to yield a neutral system and a K^+ concentration of 0.8 M in the water phase. 4 of DOPG molecules were placed in their respective crystallographic binding sites in KcsA. E118 and E120 were protonated to stabilize the open state of the channel (40).

The KcsA T75A/E71A system was built by manually introducing a corresponding mutation to the KcsA E71A system (4x KcsA monomers). To obtain the WT structure, A71 in the KcsA E71A system were reverted to a glutamate which was then protonated in line with ssNMR results (41).

As the KcsA E71A structure has 2 water molecules per monomer that establish the hydrogen bonding network behind the SF, compared to 1 in WT (5), the additional water molecules were removed accordingly. SF mutants without E71A were obtained by manually introducing G77A or T75A to this WT structure. KcsA G77A/E71A was built separately in CHARMM-GUI from E71A 5vk6 using a similar protocol, and contained in addition to the protein 33 DOPG and 87 DOPE molecules, 9315 water molecules, 134 K^+ and 117 Cl^-, resulting in an electrically neutral system with the 0.8 M concentration of K^+ in the water phase.

After building a system in CHARMM-GUI, it was equilibrated using the default 6-step protocol and CHARMM36m/TIP3P parameters (23, 42–44) provided by CHARMM-GUI to reach the temperature of 290 K and the pressure of 1 bar. After introducing necessary mutations, the systems were additionally equilibrated for up to 100 ns in the NPT ensemble at respective temperatures and pressure (in this and all the subsequent simulations kept constant by the semi-isotropic barostat Parrinello-Rahman barostat (45), and velocity rescale (v-rescale) thermostat (46)), without restraints. Periodic boundary conditions (xyz) were used. Constraints were used for bonds with H atoms (LINCS (47)). Simulation timestep was 2 fs. Lennard-Jones interactions were treated with a cutoff (forces switched to 0 from 1.0 nm to 1.2 nm in CHARMM36m, plain cutoff at 0.9 nm with long range dispersion corrections for energy and pressure in Amber14sb). Coulomb interactions were treated with PME (48) with a 1.2 nm cutoff in CHARMM36m and 0.9 nm in Amber14sb. All simulations were carried out using GROMACS 2020.6 or GROMACS 2020.7 (49).

Amber14sb/TIP3P systems with LIPID17 lipids (24, 42, 50–52) were generated from the CHARMM36m structure immediately after the initial 6-step equilibration, using the charmmlipid2amber (51, 52), GROMACS pdb2gmx, or CHARMM-GUI force field conversion tools (53). Systems with Amber14sb were then additionally equilibrated for up to 100 ns in the NPT ensemble before turning on the voltage, similar to the CHARMM36m system.

Systems with Na^+ as the permeating ion were prepared by replacing all K^+ ions with Na^+ in the structures after equilibration.

Molecular dynamics simulations with applied voltage

For production runs, a constant electric field was applied to the equilibrated structures along the *z*-axis (perpendicular to the membrane plane) to yield approximately 300 mV (or -300 mV for control simulations under negative voltage). Previously it was shown that to obtain a correct transmembrane voltage in MD simulations, the whole box size in *z* should be taken into account (54). Correspondingly, the electric field E was calculated using a formula $E = \Delta V / d_z$, where d_z is the size of the box along the *z*-axis. For each system, 10 simulation replicas were carried out with 1-2 μs per replica. All simulations we carried out are listed in *SI Table 1*.

Data analysis

To count permeation events, a custom Python script was used, kindly provided by Vytautas Gapsys (available upon request). The simulation box was divided into 4 regions - below the SF (‘1‘), in SF but below its midpoint (‘2‘), in SF above its midpoint (‘3‘), and above the SF (‘4‘). A permeation event was defined as a sequential transition 1→2→3→4 for outward permeation, and in the opposite direction for inward permeation. To calculate outward conductance, the difference between the number of outward and inward permeation events was used; accordingly, the inward conductance for systems at negative voltage was taken as the negative of that value. Presented conductance values are averages over all simulation replicas for a given system, with error bars representing 95% confidence intervals calculated using Student’s *t*-distribution.

To collect ion/water positions along the *z*-axis in SF, a custom FORTRAN code was used, available in (28). Dihedral angles were collected using the standard GROMACS toolbox. A flipped state of V76 was defined as the N-CA-C-O dihedral angle falling between -130° and -50°. For plotting the data, Python 3, matplotlib and numpy were used (55, 56). Molecular visualizations were rendered using VMD (57).

Acknowledgements and funding sources

The authors thank Sergio Pérez-Conesa and Lucie Delemotte for the initial structures of KcsA E71A, and Vytautas Gapsys for the ion permeation counting script. The authors acknowledge funding from the Deutsche Forschungsgemeinschaft (DFG, German Research Foundation) through FOR2518 ‘Dynion’ Project P5.

Figures

Figure 1

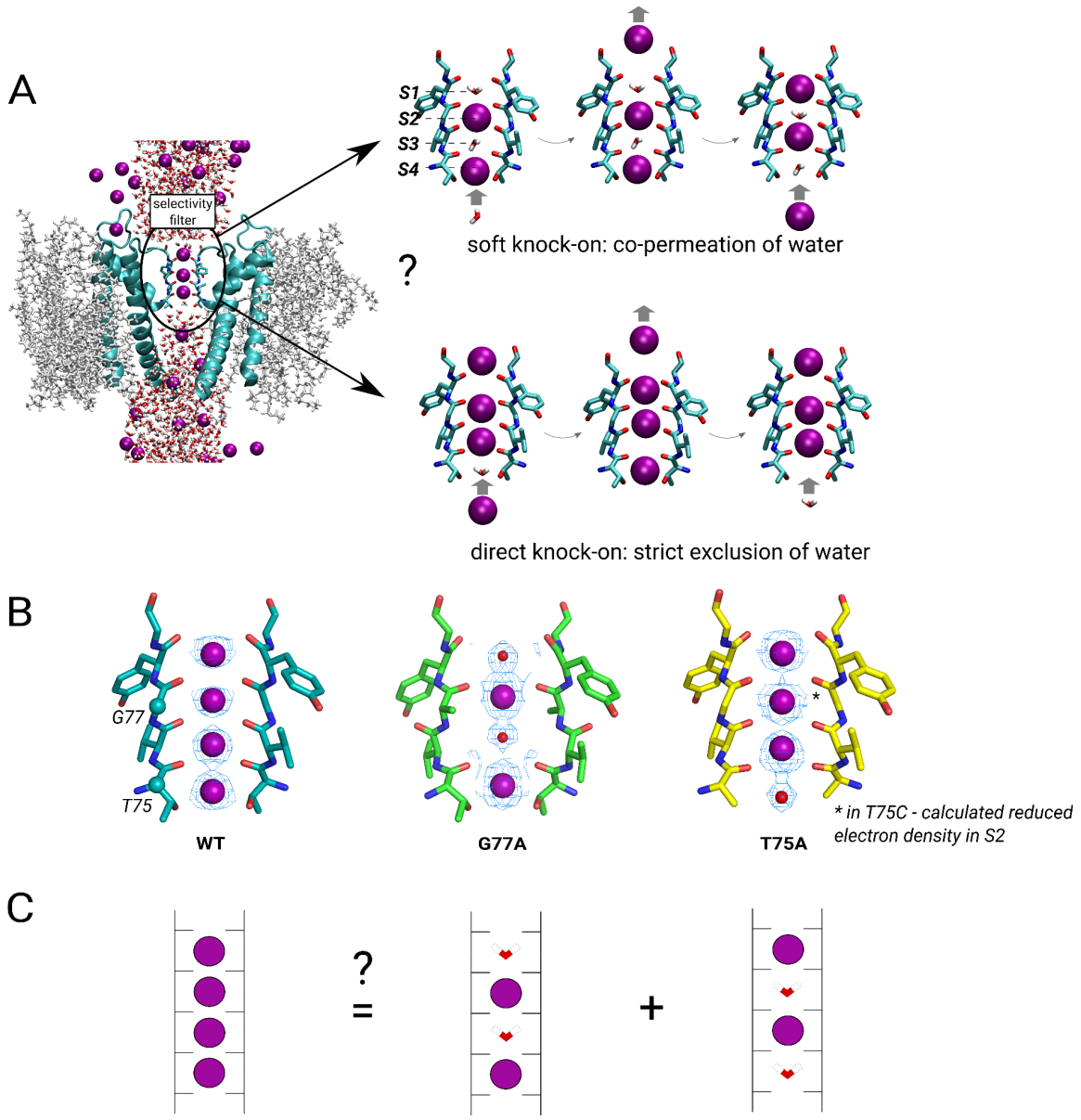

Fig. 1. Overview of ion permeation mechanisms in potassium channels. (*A*) Side view of a structure of KcsA embedded in a lipid membrane, with the highly conserved selectivity filter (SF) highlighted. K^+ ions are shown as purple spheres. On the right, main K^+/water SF configurations that occur in the two proposed permeation mechanisms, soft and direct knock-on, are shown. (*B*) Selectivity filter configurations observed in WT (PDB ID 5vk6), G77A (PDB ID 6nfu) and T75A (PDB ID 6by3) KcsA. (*C*) One possible interpretation of the fully K^+-occupied SF observed in structures of many WT potassium channels.

Figure 2

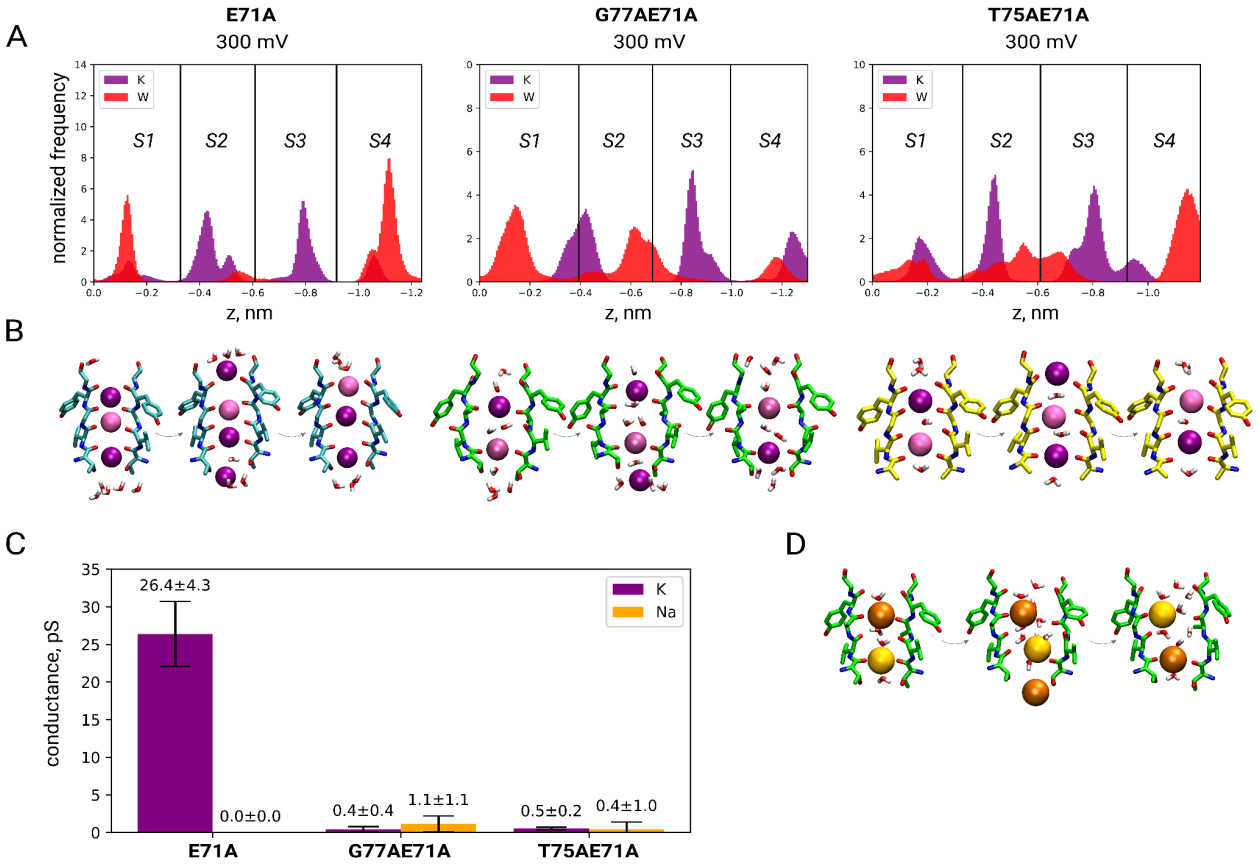

Fig. 2. (*A*) K^+/water distributions along the *z*-axis in SF of KcsA E71A, G77A/E71A and T75A/E71A from all simulation replicas with CHARMM36m at 300 mV, with (*B*) respective representative K^+/water configurations corresponding to a single K^+ permeation event. Shift to a mechanism involving co-permeation of K^+ and water is observed upon introduction of G77A and T75A mutations. (*C*) Mutations reduce the K^+ conductance and impair selectivity against Na^+ (CHARMM36m, 300mV), with (*D*) showing the representative SF configurations observed in a Na^+ permeation event in KcsA G77A/E71A.

Figure 3

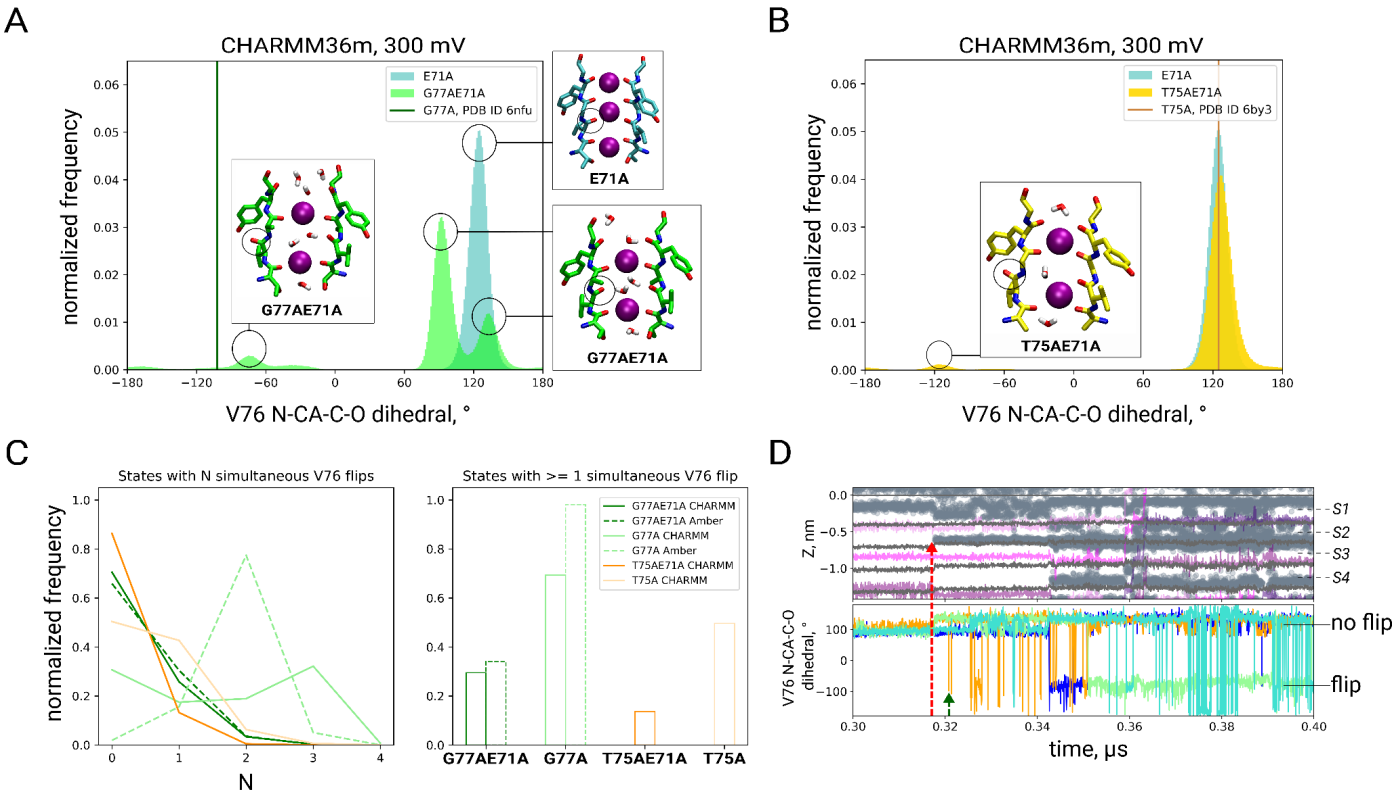

Fig. 3. SF mutants had a higher frequency of V76 carbonyl flipping, represented by V76 N-CA-C-O dihedral angle distributions for (*A*) E71A and G77A/E71A KcsA, with the dihedral angle in the G77A KcsA crystal structure indicated (PDB ID 6nfu), and (*B*) E71A and T75A/E71A KcsA, similarly indicating the dihedral angle in the T75A KcsA crystal structure (PDB ID 6by3). (*C*) Fraction of states with various numbers (N) of simultaneously flipped carbonyls (left), and the fraction of states where at least one V76 carbonyl is flipped (right). No flipping has been detected in T75A and T75A/E71A in Amber14sb. (*D*) Time traces of K^+ ions (purple lines) and water molecules (gray scatter), oxygens of SF backbone carbonyls and of threonine hydroxyls (gray lines) (up), aligned with time traces of V76 N-CA-C-O dihedral for G77A/E71A, illustrate how entrance of water into S2/S3 (red arrow) promotes V76 carbonyl flipping (green arrow).

Figure 4

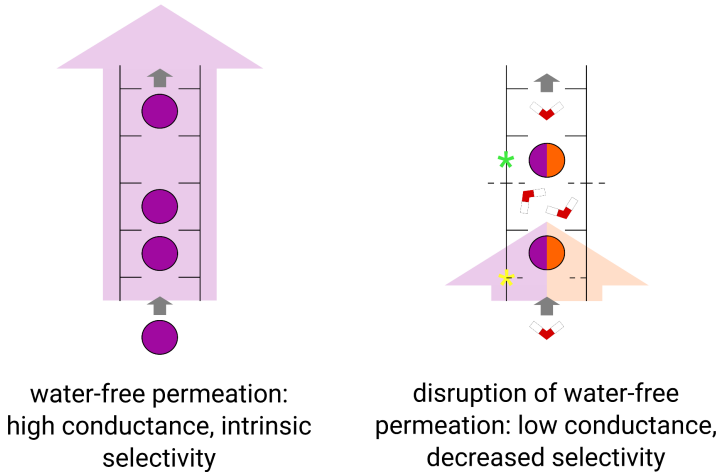

Fig. 4. Schematic view on ion permeation in WT K^+ channels (left) and the SF mutants (right) affecting either S4 (yellow) or S2 (green) K^+ binding sites. While K^+ permeation via direct knock-on is characterized by high conductance and high selectivity for K^+ ions compared to Na^+, disrupting the water-free permeation by e.g. introducing mutations to the SF impedes both permeation rates and ion selectivity. Both mutations we studied promoted flipping of V76 carbonyls (right, dashed lines in the middle), regardless of whether they affected the adjacent G77 or distant T75, which we also link to the destabilizing effect of water presence in the SF.

SI Figures

Figure S1

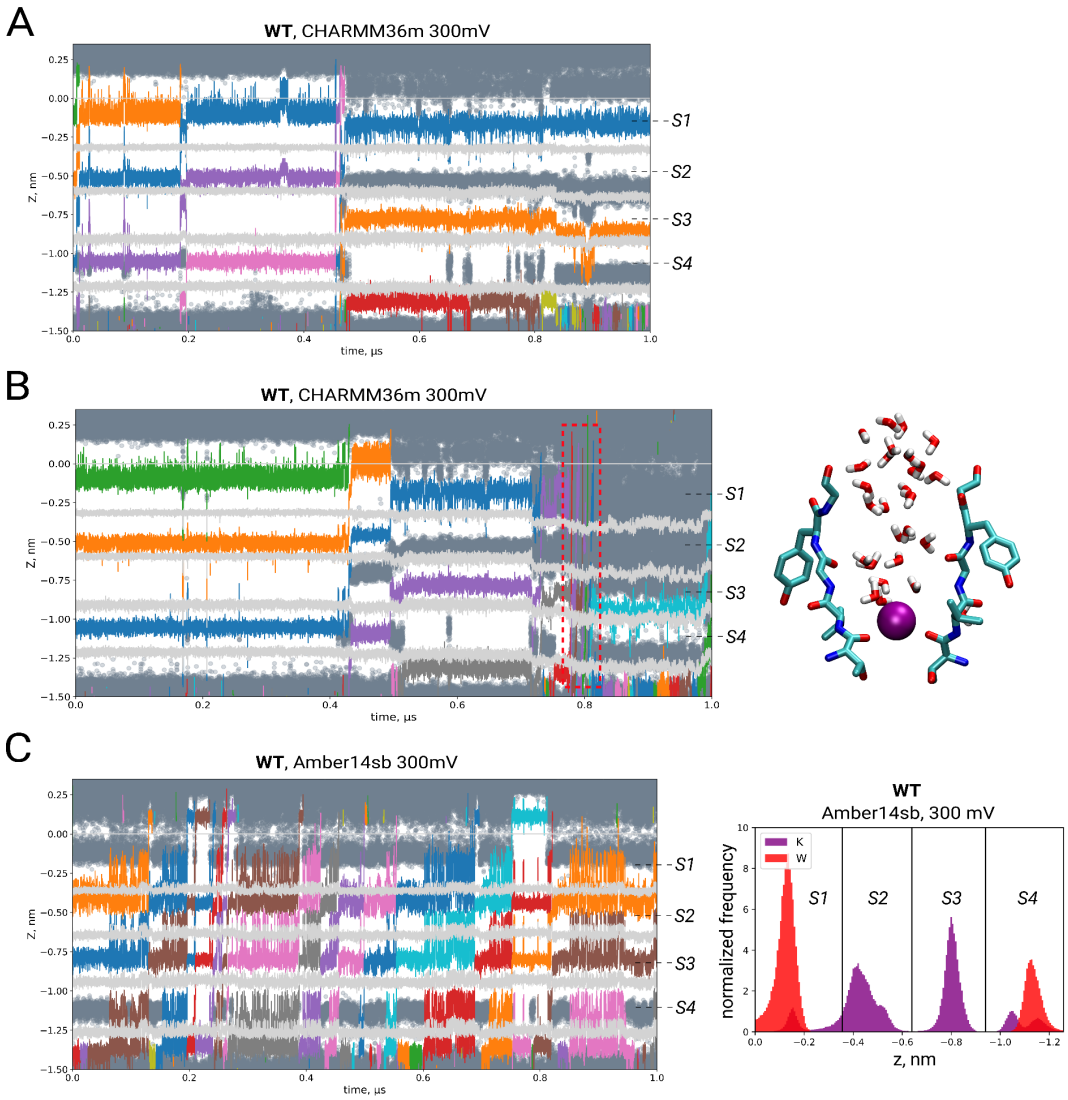

SI Fig. 1. (*A*) Traces of K^+ ions (colored lines), water molecules (dark gray scatter) and backbone carbonyl oxygens/threonine hydroxyls (light gray lines) of the SF of WT KcsA with CHARMM36m showing K^+ permeation via direct knock-on followed by entrance of water into the SF and block of further K^+ permeation. (*B*) Traces showing several events K^+/water co-permeation in one of the simulation replicas of WT KcsA with CHARMM36m (left). Those events were accompanied by a largely distorted SF with widening in the upper regions (right). (*C*) Traces showing K^+ permeation in WT with Amber14sb (left). Permeation occurred strictly via direct knock-on with water being virtually absent in the central regions of the SF, as demonstrated by K^+/water distribution from all simulation replicas (right).

Figure S2

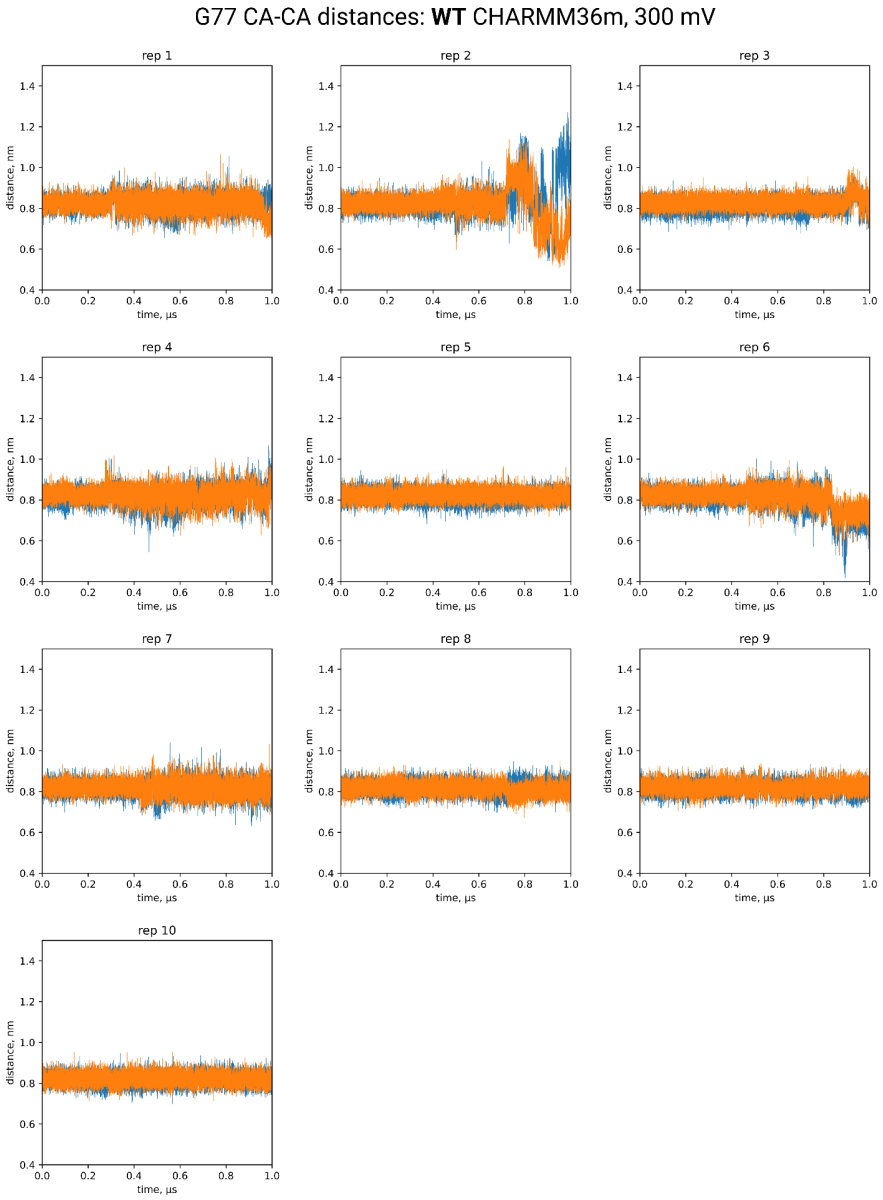

SI Fig. 2. Distance between α-carbons of G77 opposing subunits in the SF of WT KcsA. Transition to the inactivated state in WT KcsA is characterized by narrowing of the SF at G77 from ~0.8 nm to ~0.5 nm; in our simulations the WT SF was generally stable against this transition.

Figure S3

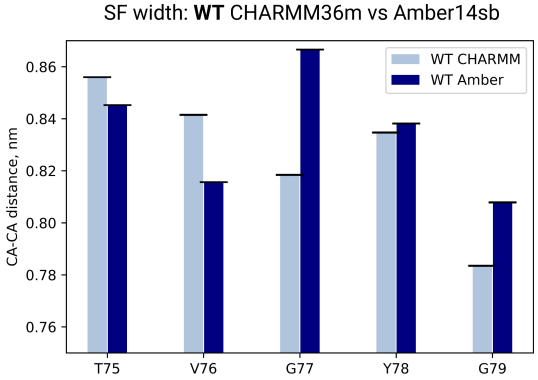

SI Fig. 3. Average distance between α-carbons of opposing subunits in the SF of WT KcsA in CHARMM36m and Amber14sb. Error bars represent 95% confidence intervals.

Figure S4

A

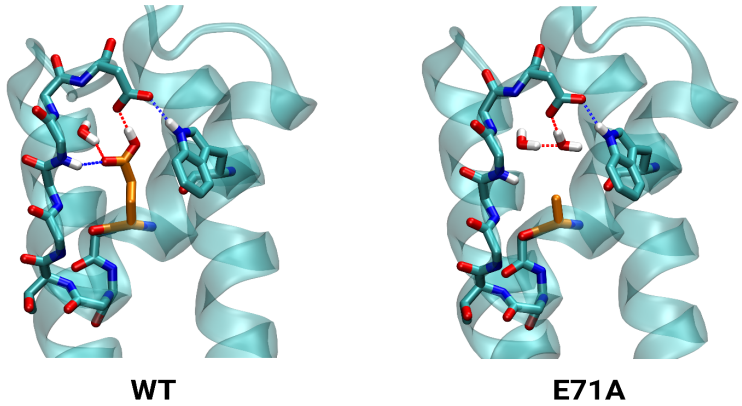

B

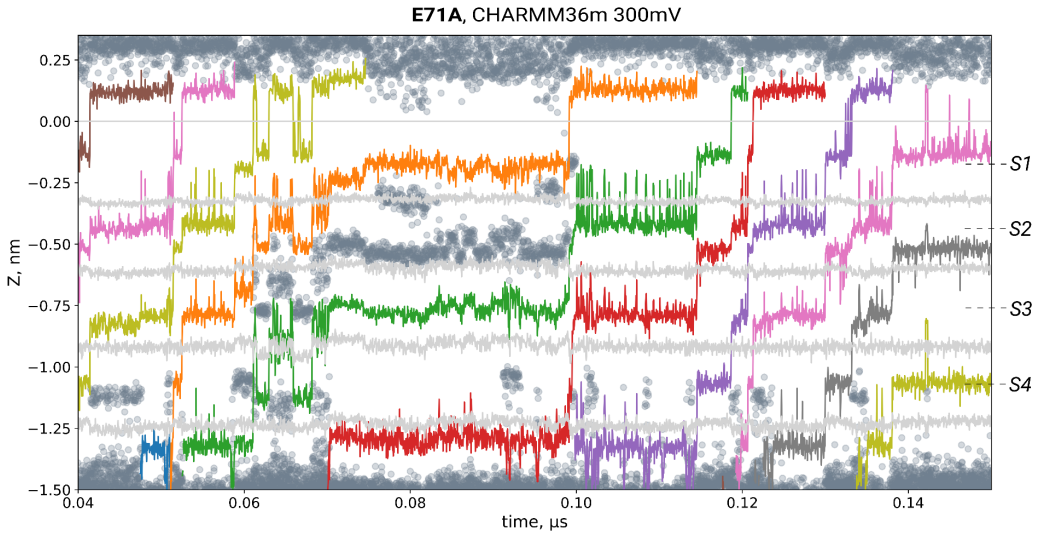

SI Fig. 4. (*A*) Hydrogen bond network behind the SF of WT KcsA (left, PDB ID 1k4c (5)) essential for SF inactivation. Mutation of E71 (orange) to alanine disrupts this hydrogen bond network (right, PDB ID 5vk6 (37)) and prevents the transition to the inactivated state. (*B*) Traces of K^+ ions (colored lines), water molecules (dark gray scatter) and backbone carbonyl oxygens/threonine hydroxyls (light gray lines) of the SF in one of simulation replicas of E71A with CHARMM36m show transient entrance of water into the SF, followed by continuation of ion permeation via water-free direct knock-on.

Figure S5

A

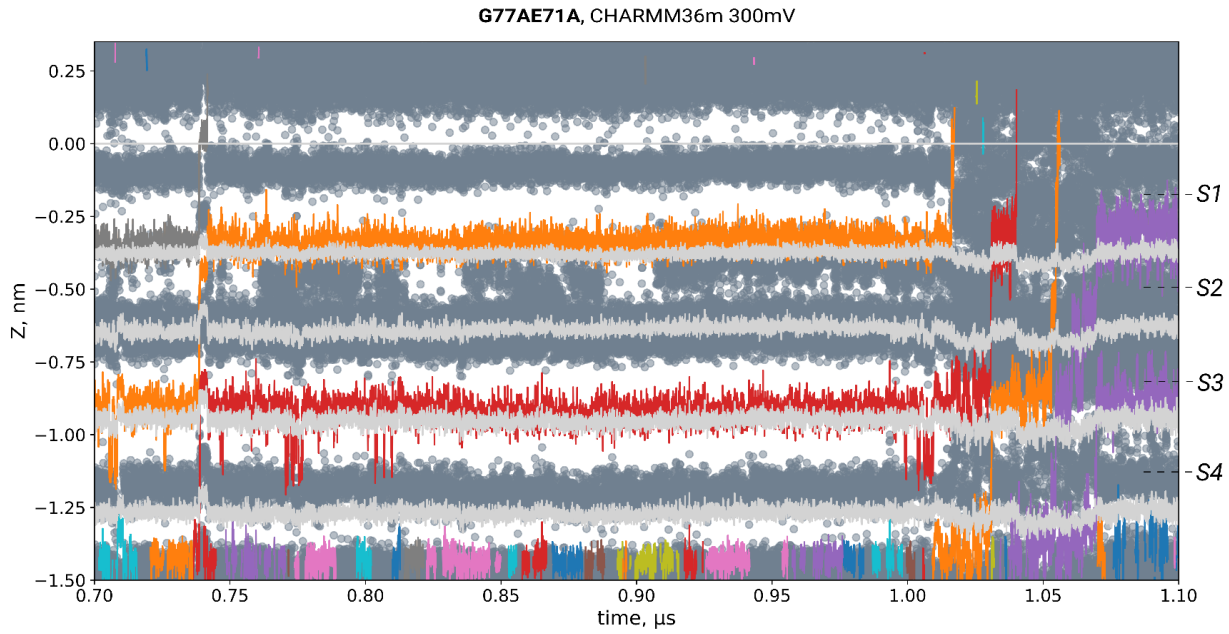

B

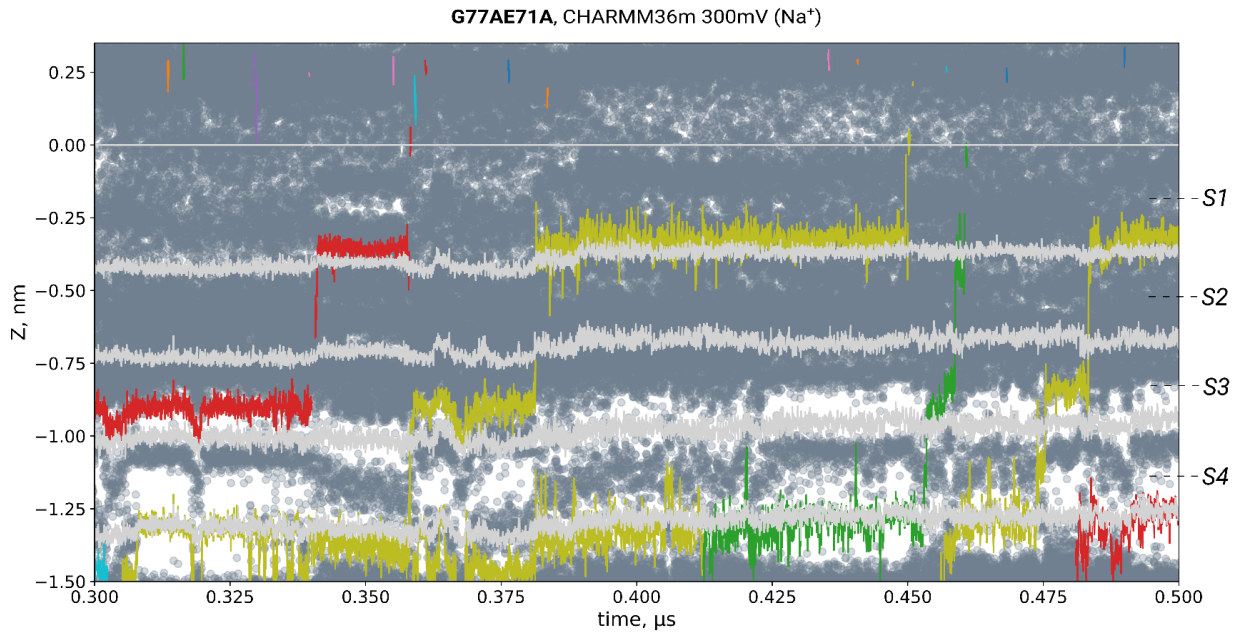

SI Fig. 5. (*A*) K^+ (colored lines), water (dark gray scatter) and backbone carbonyl oxygens'/threonine hydroxyls traces (light gray lines) in the SF of G77AE71A with CHARMM36m show permeation as jumps between KWKW-like configurations, without an intermediate WKWK. (*B*) Na^+ ion permeation in G77AE71A with CHARMM36m.

Figure S6

A

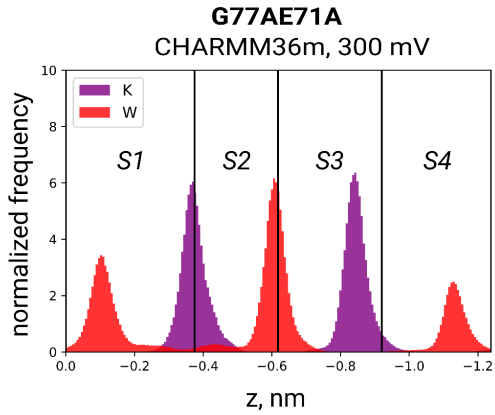

B

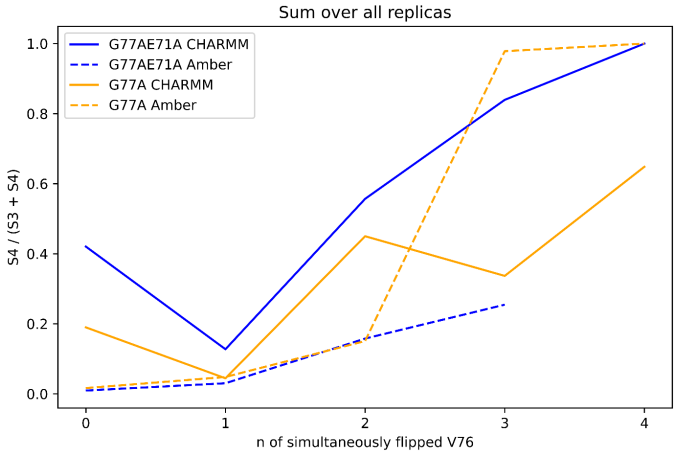

SI Fig. 6. (*A*) Distribution of K^+ and water in the SF of G77A/E71A, Amber14sb (all simulation replicas at 300 mV). (*B*) Fraction of K^+ in S4 opposed to S3 for n (1-4) simultaneously flipped V76 carbonyls for G77AE71A and G77A, showing the tendency of K^+ to prefer the crystallographic S4 when more carbonyls are flipped.

Figure S7

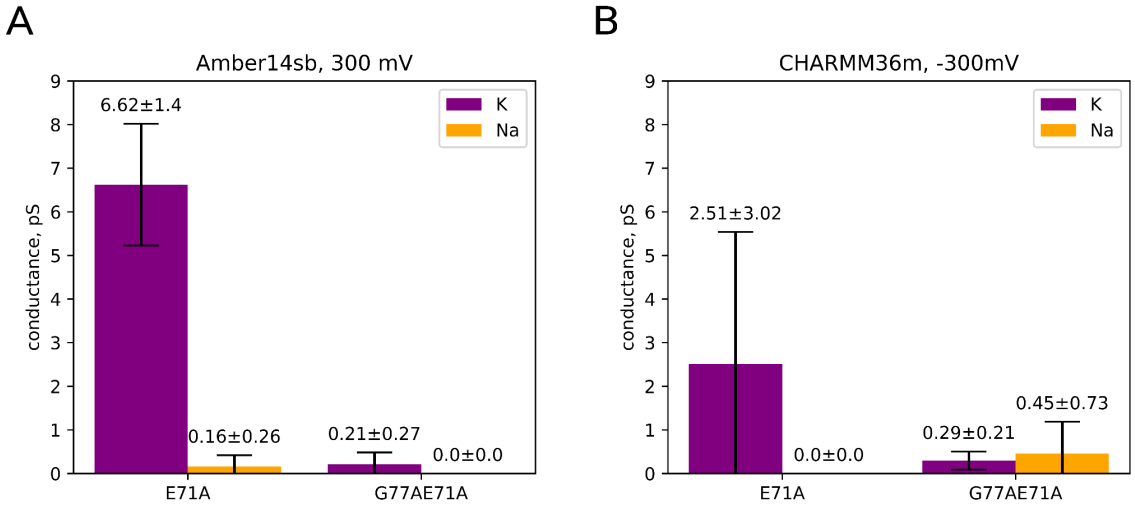

SI Fig. 7. (*A*) K^+ and Na^+ conductances of E71A and G77AE71A with Amber14sb. (*A*) K^+ and Na^+ conductances of E71A and G77AE71A with CHARMM36m at negative voltage.

Figure S8

A

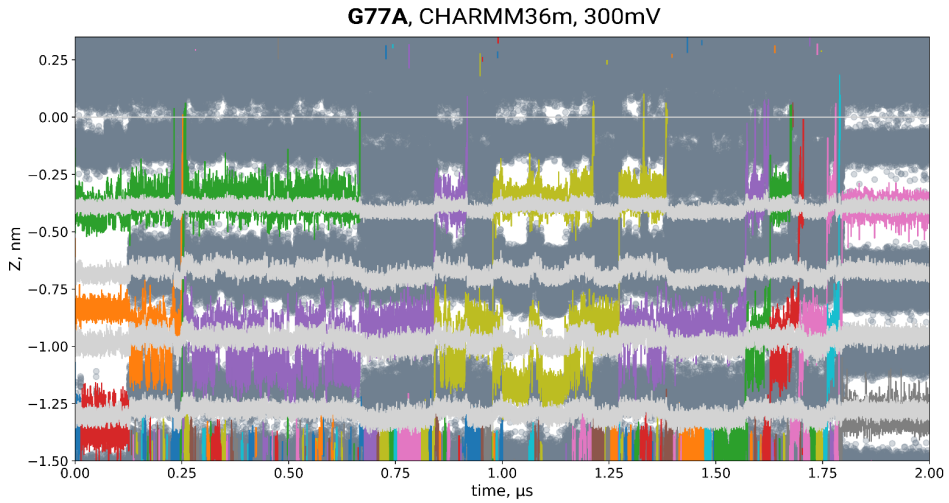

B

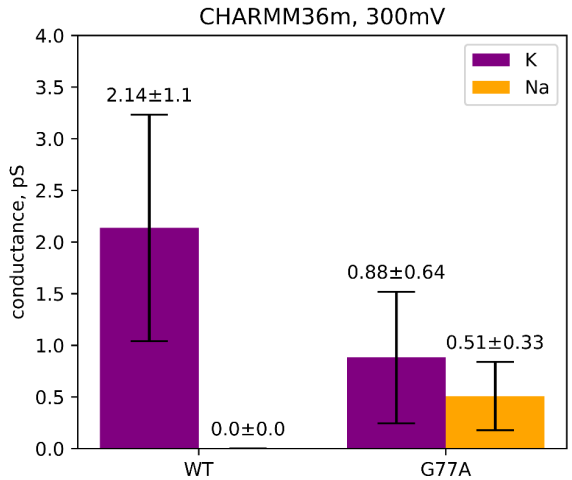

C

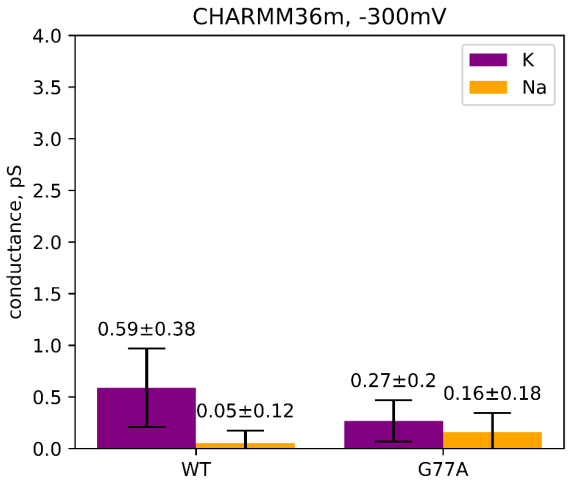

SI Fig. 8. (*A*) Co-permeation of K^+ (colored lines) and water (dark gray scatter) in the SF of G77A with CHARMM36m. Positions of backbone carbonyl oxygens and threonine hydroxyls are shown as light gray lines. K^+ and Na^+ conductances of WT and G77A with CHARMM36m at (*B*) positive and (*C*) negative voltages.

Figure S9

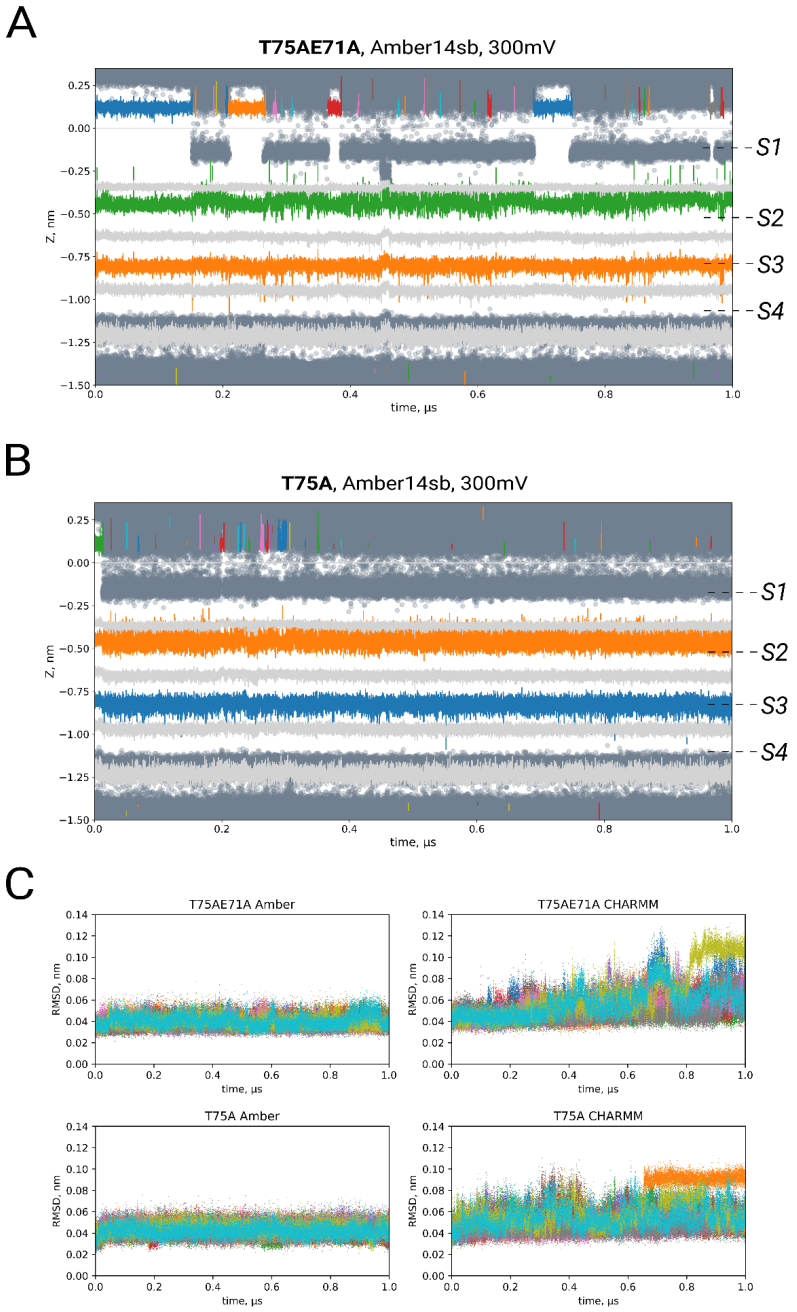

SI Fig. 9. Representative traces of K^+ (colored lines) and water (dark gray scatter) in the SF of (*A*) T75A/E71A and (*B*) T75A with Amber14sb. Positions of backbone carbonyl oxygens and threonine hydroxyls are shown as light gray lines. (*C*) RMSD of T75A/E71A and T75A SF backbone atoms, showing higher conformational stability of the SF with Amber14sb compared to CHARMM36m (300 mV, all simulation replicas).

Figure S10

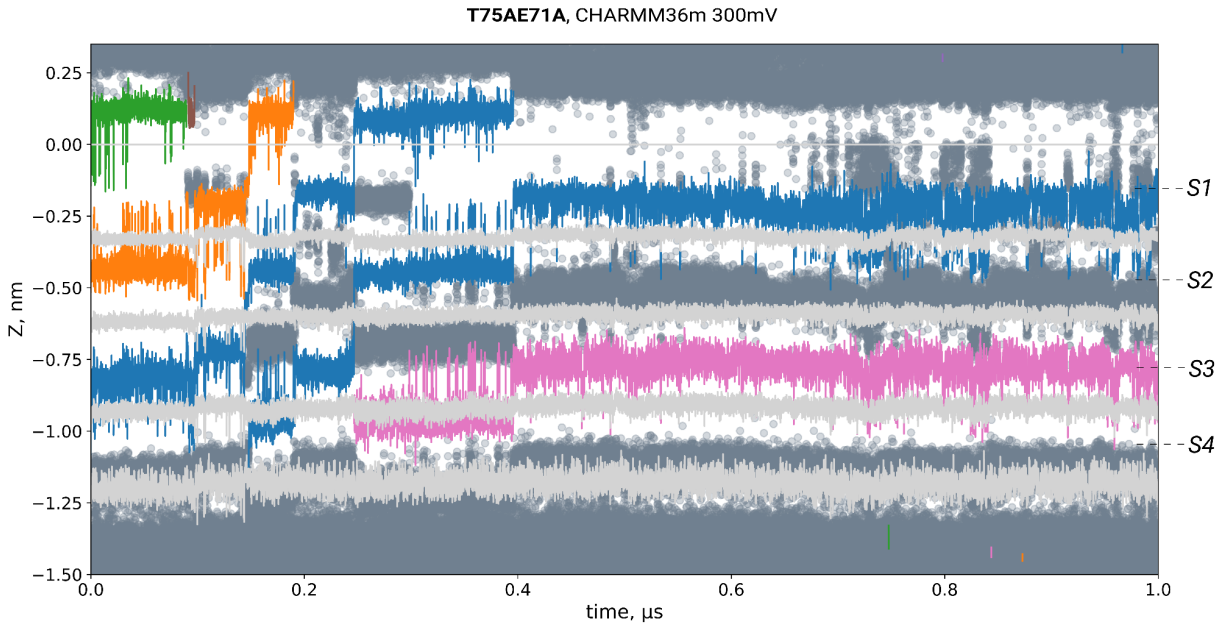

SI Fig. 10. Co-permeation of K^+ (colored lines) and water (dark gray scatter) in the SF of T75AE71A with CHARMM36m. Positions of backbone carbonyl oxygens and threonine hydroxyls are shown as light gray lines.

Figure S11

A

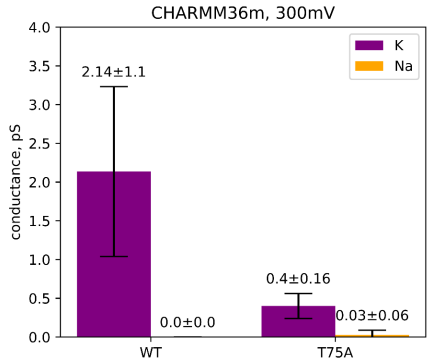

B

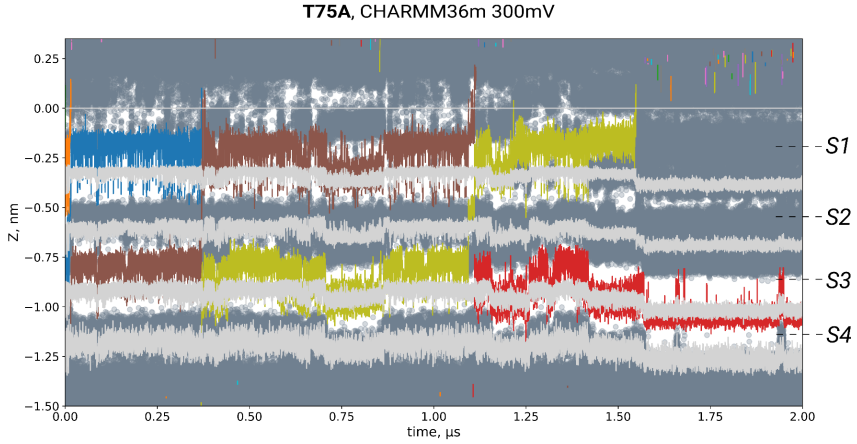

SI Fig. 11. (*A*) K^+ and Na^+ conductances of WT and T75A at 300 mV with CHARMM36m. (*B*) Traces of K^+ (colored lines), water (dark gray scatter) and backbone carbonyl oxygens'/threonine hydroxyls (light gray lines) in the SF of T75A with CHARMM36m.

Figure S12

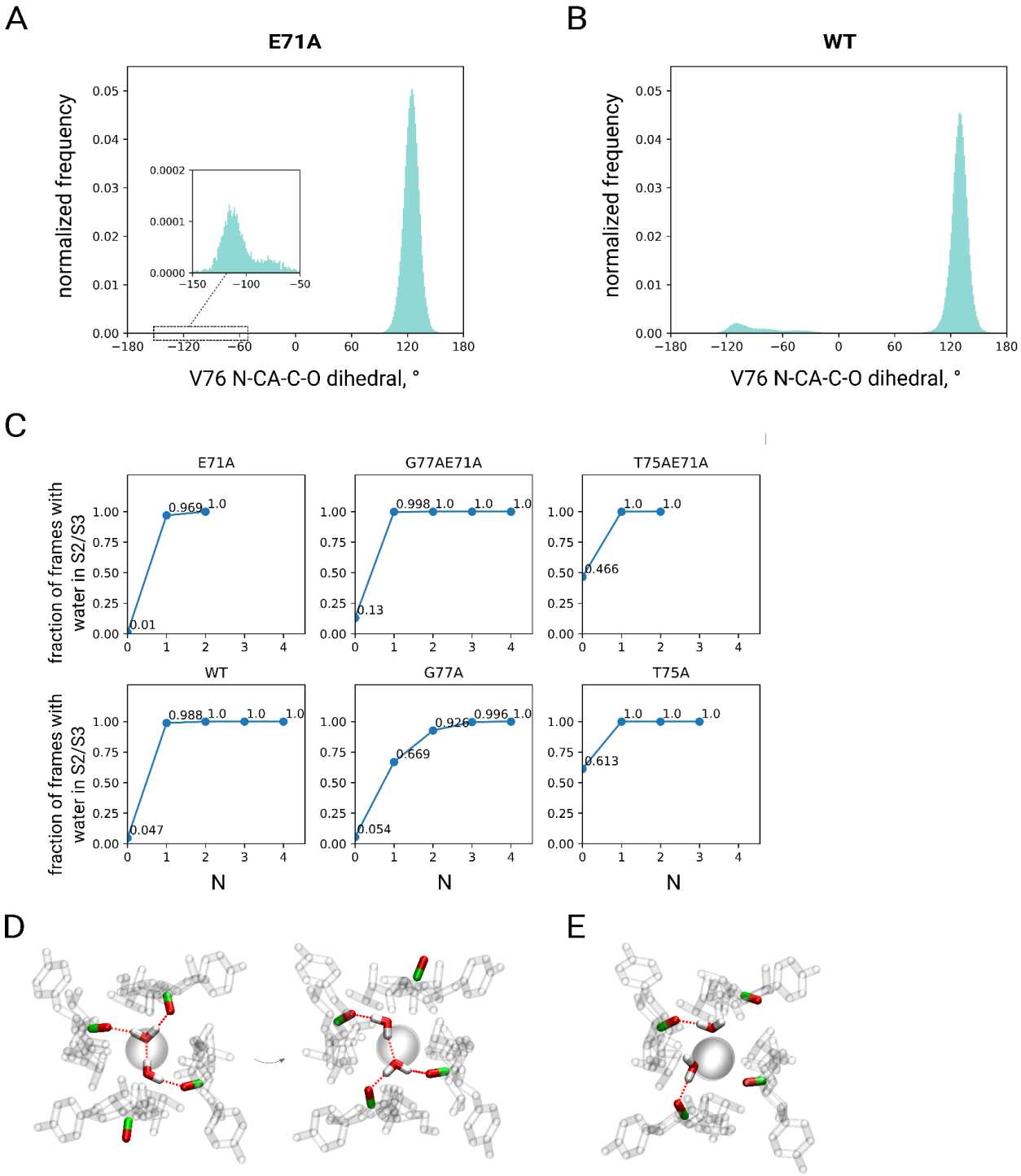

SI Fig. 12. Both E71A (*A*) and WT KcsA (*B*) show low frequency of V76 carbonyl flipping, as shown by distributions of V76 N-CA-C-O dihedrals. (*C*) Fraction of frames where water is present in S2 or S3 for each N (1-4) of simultaneously flipped carbonyls. All the data shown are for simulations with CHARMM36m. (*D*) Possible mechanism of stabilization of flipped and

non-flipped carbonyls through specific hydrogen bond networks when water molecules are present in S2 or S3. Water molecules and V76 carbonyls are opaque. Snapshots show a rearrangement of the network accompanied with a flipping of one carbonyl, and unflipping of another. (*E*) Snapshot with a non-flipped carbonyl (lower right) that is not stabilized by water hydrogen bond networks.

Figure S13

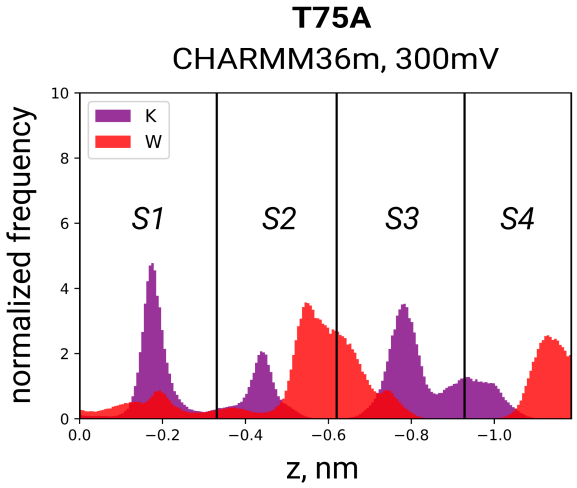

SI Fig. 13. Distribution of K^+ and water in the SF of T75A with CHARMM36m (all simulation replicas at 300 mV).

SI Table 1. List of all simulated systems.

System	Force field	Voltage	Permeant ion	Simulation time	Permeation events
E71A	CHARMM36m	300 mV	K^+	10x1 μs	494
			Na^+	10x1 μs	0
		-300 mV	K^+	10x1 μs	47
			Na^+	10x1 μs	0
	Amber14sb	300 mV	K^+	10x1 μs	124
			Na^+	10x1 μs	3
WT	CHARMM36m	300 mV	K^+	10x1 μs	40
			Na^+	10x1 μs	0
		-300 mV	K^+	10x1 μs	11
			Na^+	10x1 μs	1
	Amber14sb	300 mV	K^+	10x1 μs	81
			Na^+	10x1 μs	2
G77A/E71A	CHARMM36m	300 mV	K^+	10x~2 μs (total 19.8 μs)	15
			Na^+	10x2 μs	42
		-300 mV	K^+	10x2 μs	11
			Na^+	10x2 μs	17
	Amber14sb	300 mV	K^+	10x2 μs	4
			Na^+	10x2 μs	0
G77A	CHARMM36m	300 mV	K^+	10x2 μs	33
			Na^+	10x2 μs	19
		-300 mV	K^+	10x1 μs	5
			Na^+	10x1 μs	3
	Amber14sb	300 mV	K^+	10x1 μs	0

			Na^+	10x1 μs	0
T75A/E71A	CHARMM36m	300 mV	K^+	10x1 μs	10
			Na^+	10x1 μs	8
		-300 mV	K^+	10x1 μs	0
			Na^+	10x1 μs	0
	Amber14sb	300 mV	K^+	10x1 μs	0
			Na^+	10x1 μs	0
T75A	CHARMM36m	300 mV	K^+	10x2 μs	15
			Na^+	10x2 μs	1
		-300 mV	K^+	10x1 μs	0
			Na^+	10x1 μs	0
	Amber14sb	300 mV	K^+	10x1 μs	0
			Na^+	10x1 μs	0

References

1. B. Hille, *Ionic Channels of Excitable Membranes* (Sinauer, 2001).

2. C. M. Nimigean, J. S. Chappie, C. Miller, Electrostatic tuning of ion conductance in potassium channels. *Biochemistry* **42**, 9263–9268 (2003).

3. M. LeMasurier, L. Heginbotham, C. Miller, KcsA: it's a potassium channel. *J. Gen. Physiol.* **118**, 303–314 (2001).

4. L. Heginbotham, Z. Lu, T. Abramson, R. MacKinnon, Mutations in the K+ channel signature sequence. *Biophys. J.* **66**, 1061–1067 (1994).

5. Y. Zhou, J. H. Morais-Cabral, A. Kaufman, R. MacKinnon, Chemistry of ion coordination and hydration revealed by a K+ channel-Fab complex at 2.0 A resolution. *Nature* **414**, 43–48 (2001).

6. A. Mironenko, U. Zachariae, B. L. de Groot, W. Kopec, The Persistent Question of Potassium Channel Permeation Mechanisms. *J. Mol. Biol.* **433**, 167002 (2021).

7. Y. Zhou, R. MacKinnon, The occupancy of ions in the K+ selectivity filter: charge balance and coupling of ion binding to a protein conformational change underlie high conduction rates. *J. Mol. Biol.* **333**, 965–975 (2003).

8. J. H. Morais-Cabral, Y. Zhou, R. MacKinnon, Energetic optimization of ion conduction rate by the K+ selectivity filter. *Nature* **414**, 37–42 (2001).

9. D. A. Köpfer, *et al.*, Ion permeation in K^+ channels occurs by direct Coulomb knock-on. *Science* **346**, 352–355 (2014).

10. W. Kopec, *et al.*, Direct knock-on of desolvated ions governs strict ion selectivity in K+ channels. *Nat. Chem.* **10**, 813–820 (2018).

11. C. Alcayaga, X. Cecchi, O. Alvarez, R. Latorre, Streaming potential measurements in Ca2+-activated K+ channels from skeletal and smooth muscle. Coupling of ion and water fluxes. *Biophys. J.* **55**, 367–371 (1989).

12. C. Miller, Coupling of water and ion fluxes in a K+-selective channel of sarcoplasmic reticulum. *Biophys. J.* **38**, 227–230 (1982).

13. M. Iwamoto, S. Oiki, Counting ion and water molecules in a streaming file through the open-filter structure of the K channel. *J. Neurosci.* **31**, 12180–12188 (2011).

14. O. Rauh, U. P. Hansen, D. D. Scheub, G. Thiel, I. Schroeder, Site-specific ion occupation in the selectivity filter causes voltage-dependent gating in a viral K+ channel. *Sci. Rep.* **8**, 10406 (2018).

15. P. S. Langan, *et al.*, Anomalous X-ray diffraction studies of ion transport in K+ channels. *Nat. Commun.* **9**, 4540 (2018).

16. S. Ye, Y. Li, Y. Jiang, Novel insights into K+ selectivity from high-resolution structures of an open K+ channel pore. *Nat. Struct. Mol. Biol.* **17**, 1019–1023 (2010).

17. C. Öster, *et al.*, The conduction pathway of potassium channels is water free under physiological conditions. *Sci Adv* **5**, eaaw6756 (2019).

18. C. Tilegenova, *et al.*, Structure, function, and ion-binding properties of a K+ channel stabilized in the 2,4-ion–bound configuration. *Proceedings of the National Academy of Sciences* **116**, 16829–16834 (2019).

19. M. Zhou, R. MacKinnon, A mutant KcsA K(+) channel with altered conduction properties and selectivity filter ion distribution. *J. Mol. Biol.* **338**, 839–846 (2004).

20. K. Matulef, A. W. Annen, J. C. Nix, F. I. Valiyaveetil, Individual Ion Binding Sites in the K(+) Channel Play Distinct Roles in C-type Inactivation and in Recovery from Inactivation. *Structure* **24**, 750–761 (2016).

21. A. J. Labro, D. M. Cortes, C. Tilegenova, L. G. Cuello, Inverted allosteric coupling between activation and inactivation gates in K+ channels. *Proc. Natl. Acad. Sci. U. S. A.* **115**, 5426–5431 (2018).

22. M. G. Derebe, *et al.*, Tuning the ion selectivity of tetrameric cation channels by changing the number of ion binding sites. *Proc. Natl. Acad. Sci. U. S. A.* **108**, 598–602 (2011).

23. J. Huang, *et al.*, CHARMM36m: an improved force field for folded and intrinsically disordered proteins. *Nat. Methods* **14**, 71–73 (2017).

24. J. A. Maier, *et al.*, ff14SB: Improving the Accuracy of Protein Side Chain and Backbone Parameters from ff99SB. *J. Chem. Theory Comput.* **11**, 3696–3713 (2015).

25. J. Li, J. Ostmeyer, L. G. Cuello, E. Perozo, B. Roux, Rapid constriction of the selectivity filter underlies C-type inactivation in the KcsA potassium channel. *J. Gen. Physiol.* **150**, 1408–1420 (2018).

26. S. Furini, C. Domene, Critical Assessment of Common Force Fields for Molecular Dynamics Simulations of Potassium Channels. *J. Chem. Theory Comput.* **16**, 7148–7159 (2020).

27. W. Kopec, A. S. Thomson, B. L. de Groot, B. S. Rothberg, Driving Forces underlying Selectivity Filter Gating in the MthK Potassium Channel. *bioRxiv*, 2022.03.29.486236 (2023).

28. W. Kopec, B. S. Rothberg, B. L. de Groot, Molecular mechanism of a potassium channel gating through activation gate-selectivity filter coupling. *Nat. Commun.* **10**, 5366 (2019).

29. J. T. Brennecke, B. L. de Groot, Mechanism of Mechanosensitive Gating of the TREK-2 Potassium Channel. *Biophys. J.* **114**, 1336–1343 (2018).

30. J. Vandenberg, *et al.*, Structural Basis for Rapid Voltage Dependent Inactivation of HERG Potassium Channels (2021) https:/doi.org/10.21203/rs.3.rs-1105661/v1 (April 14, 2023).

31. X. Du, *et al.*, Loss-of-function BK channel mutation causes impaired mitochondria and progressive cerebellar ataxia. *Proceedings of the National Academy of Sciences* **117**, 6023–6034 (2020).

32. P. A. Slesinger, *et al.*, Functional effects of the mouse weaver mutation on G protein-gated inwardly rectifying K+ channels. *Neuron* **16**, 321–331 (1996).

33. P. Kofuji, *et al.*, Functional analysis of the weaver mutant GIRK2 K+ channel and rescue of weaver granule cells. *Neuron* **16**, 941–952 (1996).

34. C. M. Nimigean, C. Miller, Na+ block and permeation in a K+ channel of known structure. *J. Gen. Physiol.* **120**, 323–335 (2002).

35. A. Masotti, *et al.*, Keppen-Lubinsky syndrome is caused by mutations in the inwardly rectifying K+ channel encoded by KCNJ6. *Am. J. Hum. Genet.* **96**, 295–300 (2015).

36. T. Friesacher, *et al.*, A selectivity filter mutation provides insights into gating regulation of a K+ channel. *Commun Biol* **5**, 345 (2022).

37. L. G. Cuello, D. M. Cortes, E. Perozo, The gating cycle of a K+ channel at atomic resolution. *Elife* **6** (2017).

38. S. Jo, T. Kim, V. G. Iyer, W. Im, CHARMM-GUI: a web-based graphical user interface for CHARMM. *J. Comput. Chem.* **29**, 1859–1865 (2008).

39. J. Lee, *et al.*, CHARMM-GUI input generator for NAMD, GROMACS, AMBER, OpenMM,

and CHARMM/OpenMM simulations using the CHARMM36 additive force field. *J. Chem. Theory Comput.* **12**, 405–413 (2016).

40. B. J. Wylie, M. P. Bhate, A. E. McDermott, Transmembrane allosteric coupling of the gates in a potassium channel. *Proc. Natl. Acad. Sci. U. S. A.* **111**, 185–190 (2014).

41. M. P. Bhate, A. E. McDermott, Protonation state of E71 in KcsA and its role for channel collapse and inactivation. *Proc. Natl. Acad. Sci. U. S. A.* **109**, 15265–15270 (2012).

42. W. L. Jorgensen, J. Chandrasekhar, J. D. Madura, R. W. Impey, M. L. Klein, Comparison of simple potential functions for simulating liquid water. *J. Chem. Phys.* **79**, 926–935 (1983).

43. J. B. Klauda, *et al.*, Update of the CHARMM all-atom additive force field for lipids: validation on six lipid types. *J. Phys. Chem. B* **114**, 7830–7843 (2010).

44. D. Beglov, B. Roux, Finite representation of an infinite bulk system: Solvent boundary potential for computer simulations. *J. Chem. Phys.* **100**, 9050–9063 (1994).

45. M. Parrinello, A. Rahman, Polymorphic transitions in single crystals: A new molecular dynamics method. *J. Appl. Phys.* **52**, 7182–7190 (1981).

46. G. Bussi, D. Donadio, M. Parrinello, Canonical sampling through velocity rescaling. *J. Chem. Phys.* **126**, 014101 (2007).

47. B. Hess, H. Bekker, H. J. C. Berendsen, J. G. E. M. Fraaije, LINCS: A linear constraint solver for molecular simulations. *J. Comput. Chem.* **18**, 1463–1472 (1997).

48. T. Darden, D. York, L. Pedersen, Particle mesh Ewald: An N · log(N) method for Ewald sums in large systems. *J. Chem. Phys.* **98**, 10089–10092 (1993).

49. M. J. Abraham, *et al.*, GROMACS: High performance molecular simulations through multi-level parallelism from laptops to supercomputers. *SoftwareX* **1-2**, 19–25 (2015).

50. I. S. Joung, T. E. Cheatham 3rd, Determination of alkali and halide monovalent ion parameters for use in explicitly solvated biomolecular simulations. *J. Phys. Chem. B* **112**, 9020–9041 (2008).

51. Z. Wu, P. Biggin, *GMX_lipid17.ff: Gromacs Port of the amber LIPID17 force field* (2019) https:/doi.org/10.5281/zenodo.3562014.

52. D. A. Case, I. Y. Ben-Shalom, S. R. Brozell, D. S. Cerutti, AMBER 2018; 2018. *University of California, San* (2018).

53. J. Lee, *et al.*, CHARMM-GUI supports the Amber force fields. *J. Chem. Phys.* **153**, 035103 (2020).

54. J. Gumbart, F. Khalili-Araghi, M. Sotomayor, B. Roux, Constant electric field simulations of the membrane potential illustrated with simple systems. *Biochim. Biophys. Acta* **1818**, 294–302 (2012).

55. J. D. Hunter, Matplotlib: A 2D Graphics Environment. *Comput. Sci. Eng.* **9**, 90–95 (2007).

56. C. R. Harris, *et al.*, Array programming with NumPy. *Nature* **585**, 357–362 (2020).

57. W. Humphrey, A. Dalke, K. Schulten, VMD: visual molecular dynamics. *J. Mol. Graph.* **14**, 33–8, 27–8 (1996).